



Minimum Uplift Horizontal Acceleration of the Single-Nave Barrel Vault and the Rocking Frame

Haris Alexakis, Research Associate in Infrastructure Monitoring and Modelling, University of Cambridge, UK;
email: ca510@cam.ac.uk

Nicos Makris, Professor, Southern Methodist University, Dallas, Texas, USA and University of Patras, Greece.
Member, Office of Theoretical and Applied Mechanics, Academy of Athens; email: nmakris@smu.edu

ABSTRACT: This paper examines and compares the minimum horizontal acceleration that is needed to initiate uplift of the single-nave barrel vault and of the rocking frame which are the two most common masonry structural systems used to bridge a span. The paper concludes that regardless of the direction of the rupture of the buttresses, the single-nave barrel vault uplifts with a seismic coefficient, ε , that is always smaller than the slenderness of the buttresses, $s=b/h$. In contrast, the rocking frame always uplifts with a seismic coefficient, $\varepsilon=b/h$, regardless of the mass of its prismatic epistyle; therefore, the rocking frame has a superior seismic performance than the single-nave barrel vault.

KEYWORDS: stone arches, buttresses, articulated structures, energy methods, limit state analysis, earthquake engineering

SITE LOCATION: [Geo-Database](#)

INTRODUCTION

The planar seismic stability analysis of a masonry structure that does not sustain tension can be analyzed in two steps. Step (a) is an equivalent static-equilibrium stability analysis and deals with the calculation of the minimum horizontal acceleration, \ddot{u}_g^{up} , that is needed to rupture the structure at a minimum number of locations which are sufficient to convert the structure into a mechanism. Step (a) is a purely geometric problem which is independent of the size (scale) of the structure and depends only on its “slenderness”. Step (b) deals with the post rupturing dynamic response analysis of the hinged structure that undergoes some rocking motion and involves the solution of the nonlinear equation of motion (Oppenheim 1992); while addressing satisfactorily the impact that happens whenever the motion reverses (De Lorenzis et al. 2007). Step (b) is a purely dynamic problem that involves the participation of the rotational inertia of the articulated portions of the hinged structure; therefore, the post dynamic stability of the hinged structure depends strongly on its size (Makris 2014a,b).

This work focuses on identifying the lower hinging mechanism of the single-nave barrel vault that is a masonry arch supported on two vertical buttresses as schematically shown in Fig. 1(a,b). Accordingly, this work concentrates in addressing step (a) for the structural system shown in Fig. 1(a,b), since it is most relevant to a wide range of historic structures known as “single-nave barrel vault” churches that were built in various parts of Europe as early as a millennia ago. For instance, Fig. 2(a) shows an exterior view of the church of Agia Marina, Frenaros, Cyprus of the 15th century, and Fig. 2(b) shows an exterior and interior view of the church of Saint Catherine, Larnaca, Cyprus of the 14th century. The configuration of an arch (or vault) that is supported on buttresses is also often encountered as a substructure of more complex masonry structures, such as romanesque or gothic cathedrals and byzantine churches, medieval palaces and castles or other simpler vaulted masonry structures which have been constructed throughout the world since the conception of the masonry arch (Huerta 2006, Roca et al. 2010). The planar analysis presented in this work assumes a plane-strain condition; therefore neglects the end-effects of the front and back walls. Accordingly, the rupturing values of the seismic coefficient, ε , computed in this work represent the low limit.

The level of ground shaking that is needed to initiate rupturing as calculated in step (a) does not challenge the ultimate stability of the structure, given that the structure possesses further post-uplift dynamic stability; however, it addresses the issue of

Submitted: 22 June 2017; Published: 16 November 2018

Reference: Alexakis, H and Makris, N. (2018). *Minimum Uplift Horizontal Acceleration of the Single-Nave Barrel Vault and the Rocking Frame*, Vol.4, Issue 4, p.275-288. doi: 10.4417/IJGCH-04-04-04

locating the imminent hinges and rupturing of the masonry—an issue that is of utmost interest to the preservation efforts of cultural heritage.

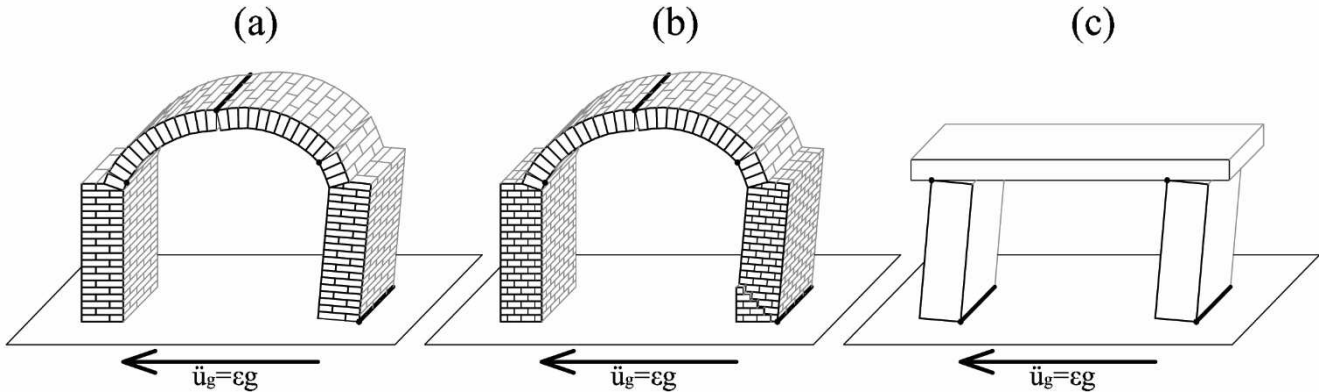


Figure 1. Single nave barrel vault subjected to a horizontal ground acceleration, $\ddot{u}_g = eg$. (a) Horizontal rupture at the base of the buttress, (b) oblique rupture, (c) the rocking frame.



Figure 2. (a) Exterior view of the church of Agia Marina, Frenaros, Cyprus (15th century) and (b) exterior and interior view of the church of Saint Catherine, Larnaca, Cyprus (14th century).

STEREOTOMY AND HINGE LOCATION

In a structure that does not sustain tension, the only seismic resisting action is its own weight. When the lateral seismic forces overcome the stabilizing gravity forces the masonry structure ruptures at a minimum number of locations creating the lower hinging mechanism. Clearly, when hinging is imminent, a masonry structure that has finite thickness may rupture in a variety of ways depending on the size of the individual stones and the configuration of the joints (Alexakis and Makris 2015). For instance, for the simplest masonry structure that is the monolithic free-standing column, there is only one joint—that is the interface at the base of the column and the location of the hinge—that is the pivot point at its base known a priori. Consequently for the monolithic, free-standing column with base, b , and height, h , step (a) introduced earlier reduces to a simple static moment equilibrium given that the minimum uplift horizontal acceleration is merely $\ddot{u}_g^{up} = g(b/h) = gtan\alpha$.

In the case of a circular arched monolith (Makris and Alexakis 2013, Alexakis and Makris 2014) with embrace angle, β , midthickness radius, R , and thickness, t , that is about to become a four-hinge mechanism, rupturing can happen in a variety of ways—say radial ruptures or vertical ruptures. When hinging is imminent, the weights of the articulated portions of the arched monolith depend on the direction of rupturing (stereotomy). Accordingly, the direction of rupturing (stereotomy) dictates the exact locations of the imminent hinges; and once the hinging mechanism has been established, one can compute the minimum horizontal acceleration needed to overcome the stabilizing gravity forces.

In the case of a masonry barrel vault, the arch atop the buttresses is constructed with voussoirs with finite size so rupturing along the radial direction is most realistic and is adopted in this study. At the same time a masonry buttress is not a monolithic column since it consists of individual stones placed roughly in horizontal courses and laid with or without mortar between

the stones. In the event that the buttress is built out of large masonry blocks the rupture may happen along the horizontal direction and uplift as a monolithic column as shown in Fig. 1(a). In the event that the buttress is built out of smaller stones and the mortar has decayed with time, the buttress is incapable to sustain any tension and eventually develops an elongation failure along the compression free region (Heyman 1992, Ochsendorf 2002, Ochsendorf et al. 2004, Makris and Alexakis 2015) as shown in Fig. 1(b).

When a buttress that supports an arch is subjected to lateral inertial loading there are two types of lateral loads. The first type of lateral load originates from the inclined thrust force due to gravity that the arch is transferring at its springing at the head of the buttress and the second type of lateral load is the lateral inertial load from the ground shaking. The thrust lines and elongation failures of masonry buttresses subjected to these two types of loads were reviewed recently by Makris and Alexakis (2015) and are summarized in Fig. 3. In this figure, b and h are the width and height of the buttress, $s=b/h$ is the slenderness, T is the resultant thrust force applied at the head of the buttress, ε and q are coefficients of the uniform and inverse triangular lateral inertial loading, $y(z)$ is the thrust line, where z is the independent variable (vertical axis) and y the dependent (horizontal axis), $t_y=T_y/(ybh)$ and $t_z=T_z/(ybh)$ are the normalized to the buttress weight horizontal and vertical components of the thrust force T , where γ is the surface force density of the buttress and finally $f(z)$ is the elongation fracture line that starts at a distance z_e from the top of the buttress. Fig. 3 indicates that the inclined thrust force from the arch on the buttress (first row) creates an elongation failure that is a straight line (Ochsendorf et al. 2004); whereas, lateral inertial loads create elongation failures that are slightly curved lines. When the profile of lateral seismic loads is assumed uniform (second row), the elongation failure line is described by an error function (Heyman 1992), which is slightly concave outwards; whereas, when the profile of the lateral seismic load is an inverted triangle (third row), the elongation failure line can be only computed numerically (Makris and Alexakis 2015) and is slightly concave inwards. The three lines shown in Fig. 3 are mathematical results based on the idealization that the buttress is a continuous monolith that does not sustain tension. In reality, a masonry buttress consists of individual stones, some larger and some smaller and the elongation failure line may look more like the one shown in Fig. 4. Accordingly, in this study we examine the minimum uplift horizontal acceleration of a single-nave barrel vault where the “downstream” buttress may rupture either at its base with a horizontal rupture as shown in Fig. 1(a) or along a straight inclined rupture as shown in Fig. 1(b).

In this paper the variational methodology advanced by Alexakis and Makris (2014) is employed to find the limit equilibrium configuration of the single-nave barrel vault shown in Fig. 1(a,b), given that the buttresses that support the arch may develop an oblique elongation failure (Heyman 1992, Ochsendorf 2002, Ochsendorf et al. 2004, Makris and Alexakis 2015).

PHYSICALLY ADMISSIBLE HINGING MECHANISMS OF A SINGLE-NAVE BARREL VAULT

Alexakis and Makris (2017) recently showed that there are only two physically admissible hinging mechanisms for the single-nave barrel vault, as shown in Fig. 5. If an arch that is capable to support its own weight is relatively slender and/or the buttresses relatively stocky, a 4-hinge lateral mechanism develops only within the arch, as shown in Fig. 5-left (mechanism I), while the buttresses do not participate in the mechanism. This is precisely the problem of identifying the limit equilibrium state of a circular masonry arch under lateral inertial and gravity loads—a problem that has been studied by Clemente (1998) and more recently by the authors (Alexakis and Makris 2014), who presented a rigorous variational formulation in an effort to liberate the limit state analysis from the need to identify the limiting thrust line. Accordingly, the exact locations of the imminent hinges and the level of horizontal ground acceleration eg that is needed to mobilize the hinging mechanism I in Fig. 5 has been presented in detail in the paper by Alexakis and Makris (2014). It is worth noting, as it was first recognized by Clemente (1998), that if the arch is subjected to a lateral load (say from the left to the right), the extreme right extrados hinge always happens at the right springing A, while the extreme left intrados hinge D may happen within the arch at a location above the left springing (“*one springing mechanism*”), or at the left springing (“*two springing mechanism*”). In that way, the location of hinge A is known, and the analysis searches for the three unknown locations of hinges B, C and D, together with the level of the lateral load that initiates the mechanism.

If an arch capable to support its own weight is relatively thick and/or the buttresses relatively slender, the location of the extrados hinge A shall be transferred to the bottom right corner of the “downstream” buttress, in analogy with the arch mechanism, and the analysis searches again for the three unknown locations of hinges B, C and D, together with the level of the lateral load that initiates the mechanisms II, shown in Fig. 5-right.

The next section applies the principle of stationary potential energy, initially employed in Makris and Alexakis (2012, 2013) and Alexakis and Makris (2013b) to calculate the exact location of the hinges and the level of the limit horizontal inertial loading, eg , for any given geometry of the single-nave barrel vault structure that does not sustain tension.

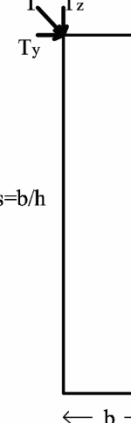
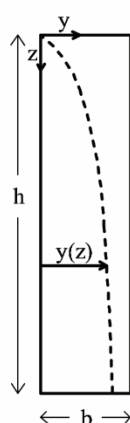
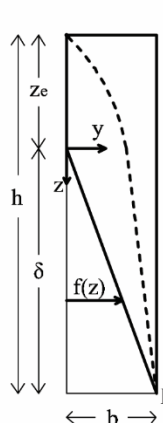
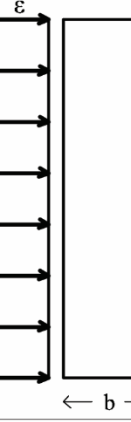
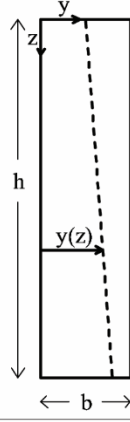
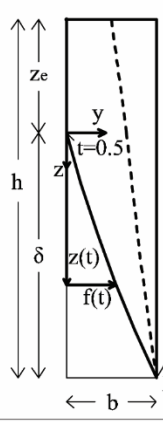
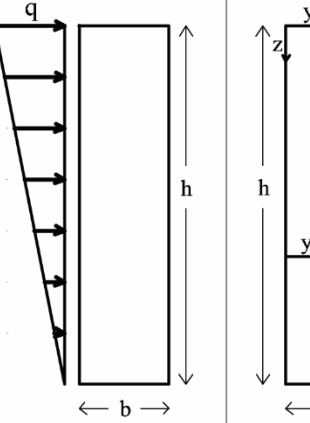
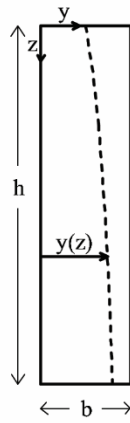
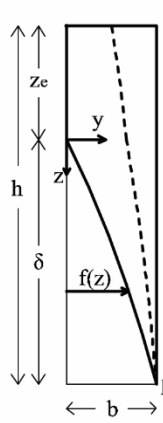
Type of Load	Equation of the Thrust Line	Elongation Failure
	 <p>$y(z) = h \left(\frac{1}{2} \frac{z}{h} \frac{s+2t_y}{\frac{z}{h} + t_z} \right)$</p> <p>Pivoting without fracturing when: $t_y = s \left(\frac{1}{2} + t_z \right)$</p>	 <p>$f(z) = s \frac{6t_y - s}{6t_y - s(1+4t_z)} z$</p> <p>$\frac{ze}{h} = \frac{4st_z}{6t_y - s}$ Ochsendorf et al. (2004)</p> <p>$t_y = \frac{s}{6} (1 + 3t_z + \sqrt{9t_z^2 + 8t_z})$</p> <p>Makris and Alexakis (2015)</p>
	 <p>$y(z) = \frac{b}{2} + \frac{\varepsilon}{2} z$</p> <p>Pivoting without fracturing when: $\varepsilon = s$</p>	 <p>$f(t) = b(1 - e^{1/4} 2t e^{-t^2})$</p> <p>$z(t) = \frac{b}{3\varepsilon} \sqrt{\pi} e^{1/4} (\text{erf}(1/2) - \text{erf}(t))$</p> <p>$\varepsilon = 0.7282s$ Heyman (1992)</p> <p>$\frac{ze}{h} = 0.4578$</p>
	 <p>$y(z) = \frac{b}{2} + \frac{q(3h-z)z}{6h}$</p> <p>Pivoting without fracturing when: $\varepsilon = \frac{3}{2}s$</p>	 <p>$f(z), q \text{ and } \delta \text{ are computed numerically}$</p> <p>$q = 0.8884s$</p> <p>$\frac{ze}{h} = 0.4396$</p> <p>Makris and Alexakis (2015)</p>

Figure 3. Thrust lines, fracture lines and expressions of the critical loads according to elongation failure of masonry buttresses with slenderness $s=b/h$ when subjected to three different loading patterns.

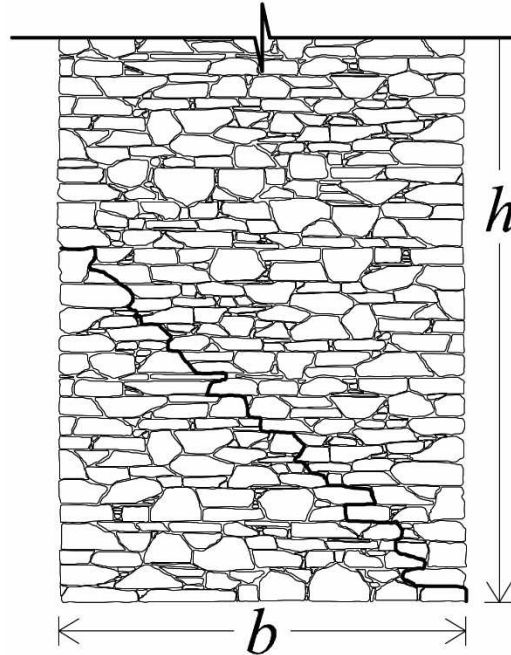


Figure 4. Schematic of elongation failure of a buttress with variable stone size and nearly-zero tensile strength at the joints.

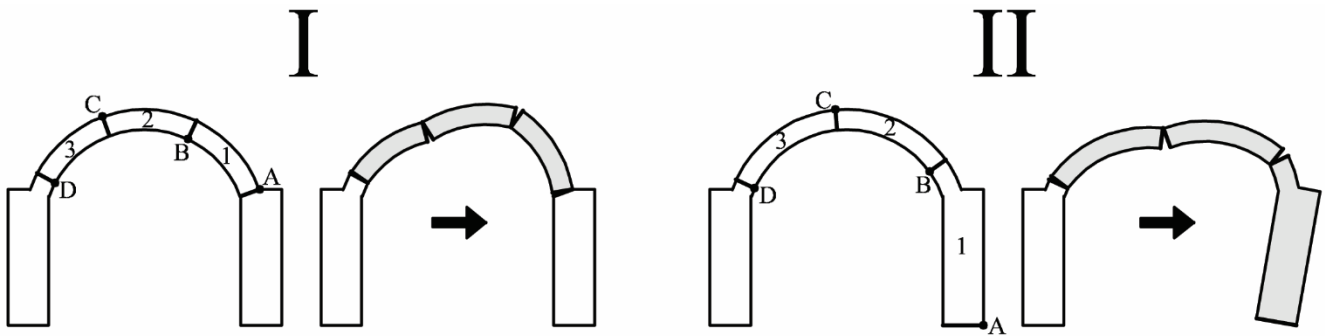


Figure 5. Admissible hinging mechanisms for buttresses that are allowed to develop horizontal ruptures.

MECHANISM II (SEMI-GLOBAL MECHANISM) THAT INITIATES A HORIZONTAL RUPTURE AT THE BASE OF THE BUTTRESS

With reference to Fig. 6-right, consider a circular arch with embrace angle, β , mid-thickness radius, R , and thickness, t , that is supported on two rectangular buttresses with height, h , and width, b . The structure is subjected to a constant horizontal ground acceleration eg (say from the left to the right). Prior to hinging, the structure translates as a rigid body; therefore, the lateral inertial loading will assume a profile proportional to the vertical distribution of the mass.

Moment equilibrium of segment 2 (segment BC) about hinge C gives

$$-\varepsilon W_2[(R + \frac{t}{2})\sin\phi_2 - y_2] + W_2[x_2 - (R + \frac{t}{2})\cos\phi_2] + T_{Bx}[(R + \frac{t}{2})\sin\phi_2 - (R - \frac{t}{2})\sin\phi_1] - T_{By}[(R - \frac{t}{2})\cos\phi_1 - (R + \frac{t}{2})\cos\phi_2] = 0 \quad (1)$$

In Eq. (1), T_{Bx} and T_{By} are the cartesian components of the unknown thrust force T_B acting at hinge B (Fig. 6 top-center), while W_2 , x_2 and y_2 are the weight and the cartesian coordinates of the center of gravity of segment 2, which are functions of the unknown rupture locations ϕ_1 and ϕ_2 (Alexakis and Makris 2017). Moment equilibrium of the combined segment 2-3 (segment BCD) about hinge D gives

$$\varepsilon W_{2-3}[y_{2-3} - (R - \frac{t}{2})\sin\phi_3] + W_{2-3}[x_{2-3} - (R - \frac{t}{2})\cos\phi_3] - T_{Bx}[(R - \frac{t}{2})\sin\phi_1 - (R - \frac{t}{2})\sin\phi_3] - T_{By}[(R - \frac{t}{2})\cos\phi_1 - (R - \frac{t}{2})\cos\phi_3] = 0 \quad (2)$$

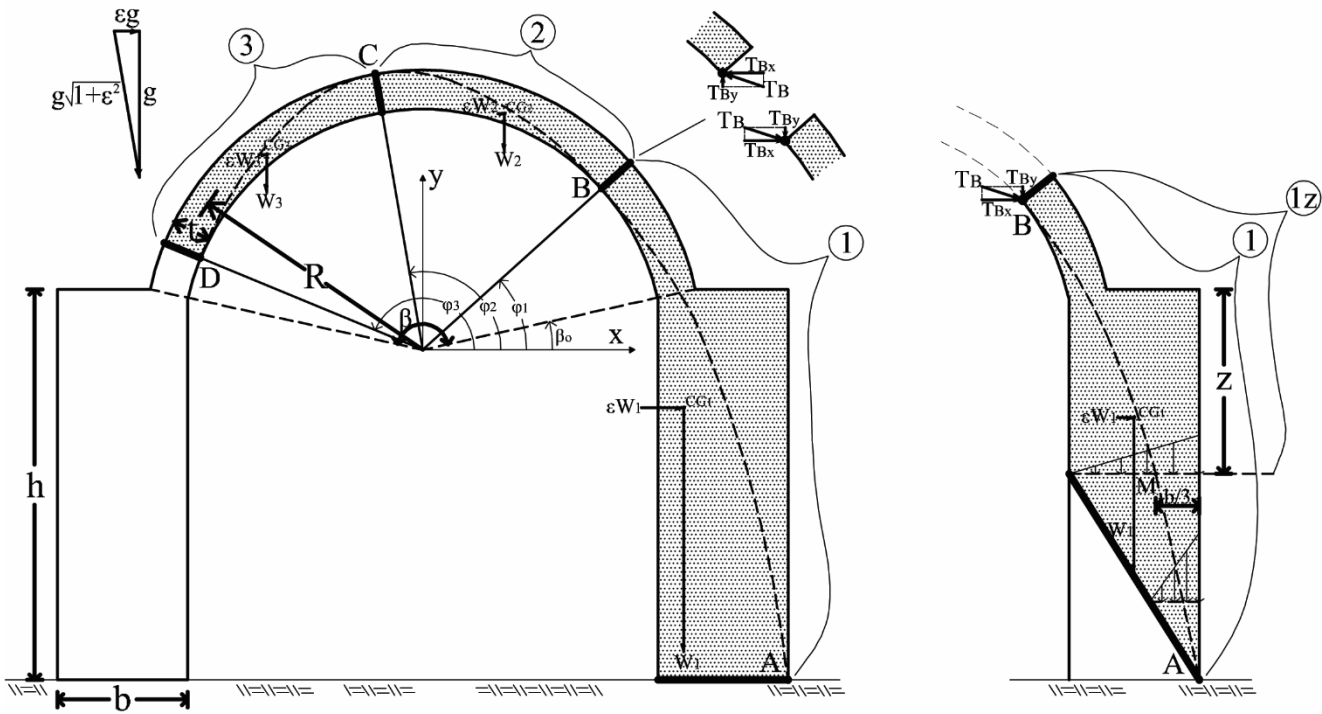


Figure 6. Formation of a four-hinge mechanism for the case where the buttresses are allowed to develop horizontal ruptures (right) or a straight oblique elongation failure (left)

In Eq. (2), W_{2-3} , x_{2-3} and y_{2-3} are the weight and the cartesian coordinates of the center of gravity of the combined segment 2-3, which are functions of the unknown rupture locations φ_1 and φ_3 (Alexakis and Makris 2017). Moment equilibrium of segment 1 (segment AB) about hinge A gives

$$\varepsilon W_1 [y_1 + h - (R + \frac{t}{2}) \sin \beta_o] - W_1 [(R - \frac{t}{2}) \cos \beta_o + b - x_1] + T_{Bx} [(R - \frac{t}{2}) \sin \phi_1 + h - (R + \frac{t}{2}) \sin \beta_o] - T_{By} [(R - \frac{t}{2}) \cos \beta_o + b - (R - \frac{t}{2}) \cos \phi_1] = 0 \quad (3)$$

In Eq. (3), $\beta_o = (\pi - \beta)/2$ is the angle that forms the springing with the horizontal axis and W_1 , x_1 and y_1 are the weight and the cartesian coordinates of the center of gravity of segment 1, which are functions of the unknown rupture location φ_1 (Alexakis and Makris 2017).

Substitution of Eqs. (1) and (2) into Eq. (3) eliminates the unknown force components T_{Bx} and T_{By} and yields a transcendental equation which involves the geometric parameters β , t/R , b/R , h/R , the rupture locations φ_1 , φ_2 , φ_3 and the seismic coefficient ε . In the event of a demand assessment analysis (i.e., find the level of loading that a given structure can sustain) the geometry of the buttressed arch is given and the analysis searches for the seismic coefficient ε that initiates the hinge mechanism. The solution of the above mentioned transcendental equation can then be expressed in the form

$$\varepsilon = f(\phi_1, \phi_2, \phi_3) \quad (4)$$

Our analysis proceeds with the application of the principle of stationary potential energy, which states that the geometrically admissible hinged mechanism is in an equilibrium state if and only if the total potential energy of the system is stationary ($\delta V=0$). Alexakis and Makris (2017) showed that the total potential energy, V , can be expressed as a function of the three unknown locations φ_1 , φ_2 and φ_3 , and is stationary when (Shames and Dym 1985, among others)

$$\frac{\partial V(\phi_1, \phi_2, \phi_3)}{\partial \phi_j} = \frac{\partial f(\phi_1, \phi_2, \phi_3)}{\partial \phi_j} = \frac{\partial \varepsilon}{\partial \phi_j} = 0, \quad j \in \{1, 2, 3\} \quad (5)$$

Eq. (4) together with the three equations from the expression (5) ($j=1,2,3$) offer a 4x4 system that can be solved numerically and calculates the four unknowns $\varepsilon, \varphi_1, \varphi_2, \varphi_3$ for a given geometry of the structural system ($\beta, t/R, b/R, h/R$). In addition, the following boundary conditions must be satisfied for mechanism II:

$$\beta_o \leq \varphi_1 < \varphi_2 < \varphi_3 \leq \pi - \beta_o \quad (6)$$

Fig. 7 plots the seismic coefficient ε as a function of the arch thickness t/R for three values of the buttress height $h/R=1, 1.5$ and 2 that correspond to the top, center and bottom graph respectively, for three values of the buttress width $b/R=0.25, 0.5$ and 0.75 and for four values of the embrace angle $\beta=180^\circ, 155^\circ, 125^\circ$ and 90° with dark solid line, gray solid line, dark dashed line and gray dashed line respectively. Isolated symbols correspond to Discrete Element Method results discussed later.

The lines with the positive slope correspond to the arch mechanism (mechanism I in Fig. 5) which is mobilized for relatively thin arches (low t/R). Clearly, in this mechanism the dominant parameter is the embrace angle of the arch. Smaller embrace angles increase considerably the seismic resistance of the arch. For the mobilization of mechanism I the geometry of the buttress is immaterial; therefore, the same lines appear at the top, center and bottom graphs of Fig. 7.

If the arch is relatively thick, mechanism II (Fig. 5) is first mobilized, which corresponds to the slightly horizontal branches. Clearly in this mechanism there is a small dependence on the arch geometry ($\beta, t/R$), while the dominant parameters are the dimensions of the buttress. For example, a slight increase of the buttress width might result in a significant increase of the seismic resistance. Tall slender buttresses that support a masonry arch, commonly found in historic structures (e.g. the nave of cathedrals) are more likely to rupture, even with relatively low peak ground acceleration.

This behavior is reminiscent to the behavior of the rocking frame which consists of two free standing columns (buttresses) capped with a rigid beam (epistyle) as shown in Fig. 1(c). The seismic response of the rocking frame was recently studied in depth by Makris and Vassiliou (2013, 2014) and it was shown that the uplift acceleration is $\ddot{u}_g^{up}=g(b/h)$, where, b , and, h , are the width and height of the vertical elements. When observing the results offered in Fig. 7, every family of lines that correspond to a given b/R is for a slenderness value of the buttress $b/h=(b/R)(R/h)$. Accordingly, the three graphs (a), (b) and (c) shown in Fig. 7 indicate that the single-nave barrel vault hinges always at a lower value of the seismic coefficient that is capable to initiate uplift of the rocking frame, that is $\varepsilon=b/h$.

It is worth mentioning that the structural system of the single-nave barrel vault was known to the ancient Greek builders as documented by the entrance arched structures to the stadium of ancient Olympia and Nemea shown in Fig. 8 (Alexakis and Makris 2013a). Nevertheless, the arch was not used by ancient Greek builders to bridge the span of consecutive columns appearing in the peristyle of Temples (Fig. 9(a)) as done later in history in the architecture of other civilizations (see for instance Fig. 9(b,c)). Perhaps the superior seismic performance of the rocking frame compared to that of the single-nave barrel vault explains the choice of ancient Greek builders to use massive prismatic epistyles to bridge the span of consecutive columns rather to build masonry arches as was done later in history.

The first five columns of Table 1 present indicative values of the seismic coefficient ε and the rupture locations φ_1, φ_2 and φ_3 , for a single-nave barrel vault with buttress height $h/R=1.5$ and width $b/R=0.5$, for the case where the buttress is allowed to develop horizontal rupture. The arch thickness t/R is ranging from 0.025 to 0.25, and the embrace angle β from 90° to 180° . Gray-shaded rows with values in italic correspond to mechanism I (arch mechanism), while the rest correspond to mechanism II. As the embrace angle, β , is increasing, very thin arches are not capable to sustain their own weight and the corresponding rows have been omitted. Values in bold correspond to the case where angles φ_1 or φ_3 indicate rupture exactly at the right or left springing of the arch. The last column of Table 1 presents the uplift acceleration of a rocking frame with buttresses of corresponding slenderness, which is always higher than the uplift acceleration of the single-nave barrel.

The Accompanying Datasheet of this paper presents values of the seismic coefficient ε and the rupture locations φ_1, φ_2 and φ_3 , for all nine buttress geometries of Fig. 7 ($h/R=1, 1.5, 2$ combined with $b/R=0.25, 0.5, 0.75$).

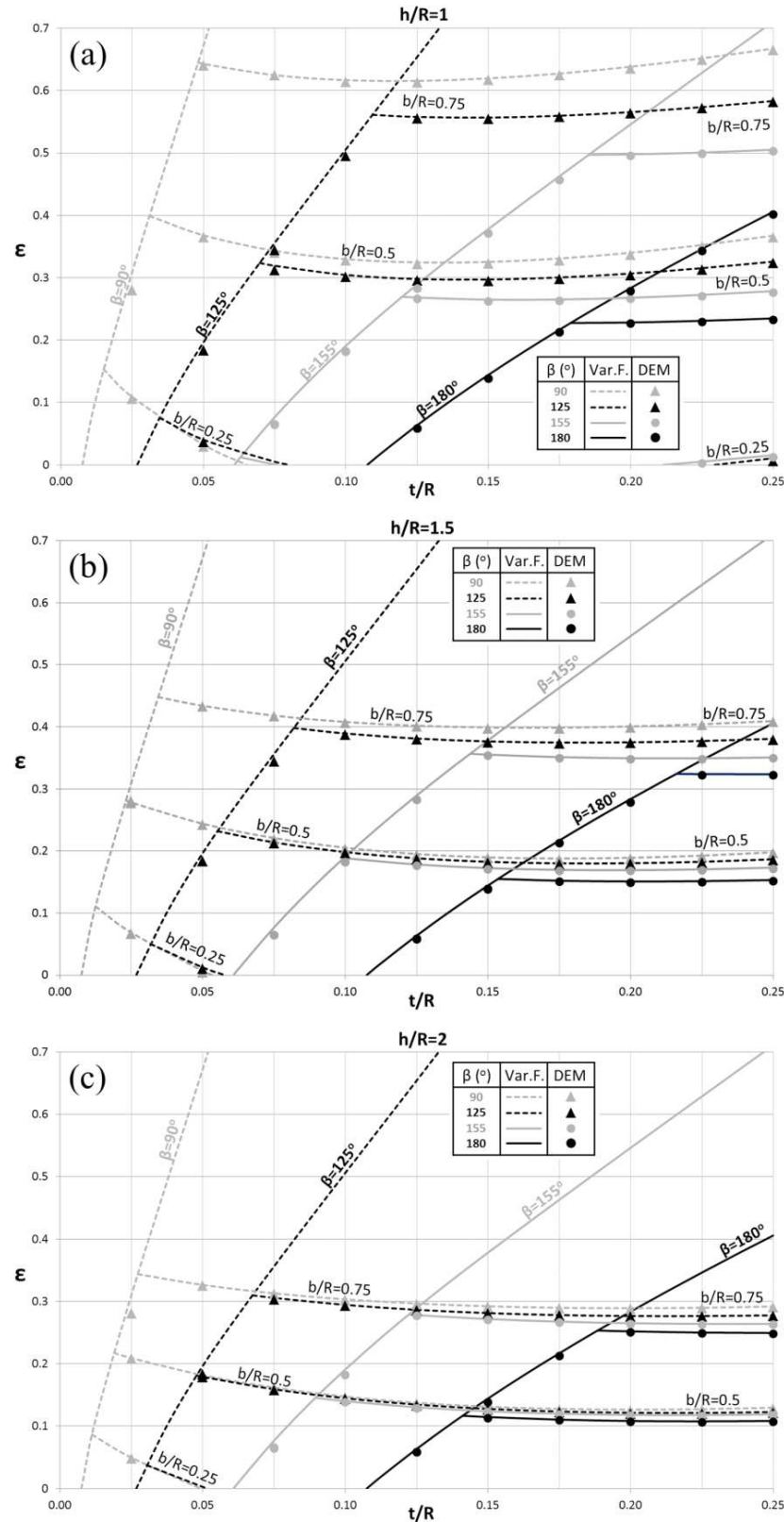


Figure 7. Seismic coefficient ϵ for different geometries of the single-nave barrel vault with buttresses that are allowed to develop horizontal ruptures. Lines: Results from the variational formulation. Isolated symbols: Results from the Discrete Element Method (DEM).



Figure 8. Views of ancient Greek masonry vaults. Left: entrance arch to the stadium of ancient Olympia. Right: the tunnel entrance of the stadium of ancient Nemea.

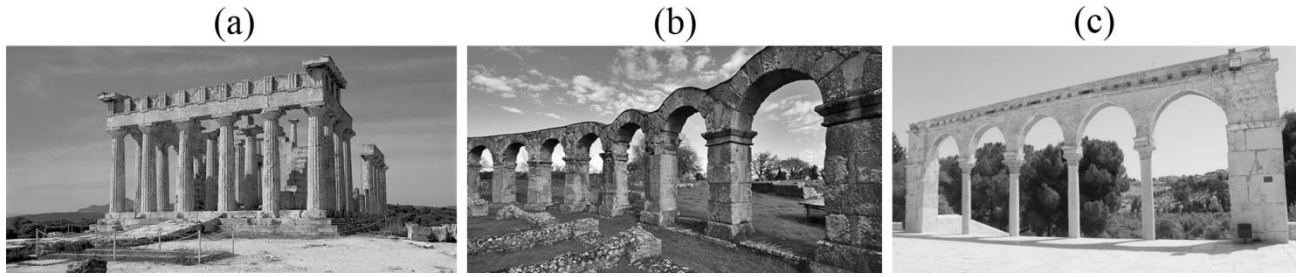


Figure 9. (a) View of the Temple of Aphaia in Aegina, Greece. Its monolithic, free-standing columns support massive prismatic epistyles and the frieze atop, and the entire rocking frame remains standing for more than 2500 years. (b) Colonnade of the Roman Theatre of Ferento, Italy built during the 1st century AD. (c) The Eastern Colonnade of Dome of the Rock Islamic shrine, Jerusalem (11th century).

MECHANISM II (SEMI-GLOBAL MECHANISM) THAT INITIATES AN OBLIQUE ELONGATION RUPTURE ALONG THE BUTTRESS

A masonry buttress is not a monolithic column since it consists of individual stones placed roughly in horizontal courses and laid with or without mortar between the stones. In the event that the buttress is built out of large masonry blocks the rupture may happen along the horizontal direction and mobilize mechanism II shown in Fig. 5. In the event that the buttress is built out of smaller stones and the mortar has decayed with time, the buttress is incapable to sustain any tension and eventually develops an elongation failure along the compression free region (Heyman 1992, Ochsendorf 2002, Ochsendorf et al. 2004, Makris and Alexakis 2015).

Assuming a triangular stress distribution along the horizontal layers of the buttress and with reference to Fig. 6-right, the compression free area originates at distance z from the head of the buttress, where the base of the triangular stress distribution is equal to the width of the buttress, b . Accordingly, point M is the intersection point of the base of the triangular stress distribution and the trust line, located at distance $b/3$ from the external side of the buttress.

The most critical fracture passes through the bottom corner of the buttress, as shown in Fig. 6-right (see also Heyman 1992, Ochsendorf 2002, Ochsendorf et al. 2004, Makris and Alexakis 2015). The distance z can be calculated by taking moment equilibrium of segment 1z about point M (see Fig. 6-right), which gives

$$\varepsilon W_{1z} [y_{1z} + z - (R + \frac{t}{2}) \sin \beta_o] - W_{1z} [(R - \frac{t}{2}) \cos \beta_o + \frac{2b}{3} - x_{1z}] + T_{Bx} [(R - \frac{t}{2}) \sin \phi_1 + z - (R + \frac{t}{2}) \sin \beta_o] - T_{By} [(R - \frac{t}{2}) \cos \beta_o + \frac{2b}{3} - (R - \frac{t}{2}) \cos \phi_1] = 0 \quad (7)$$

In Eq. (7), W_{1z} , x_{1z} and y_{1z} are the weight and the cartesian coordinates of the center of gravity of segment 1z (Alexakis and Makris 2017).

Table 1. Indicative values of the seismic coefficient ε and the rupture locations φ_1 , φ_2 and φ_3 , for a single-nave barrel vault with buttress height $h/R=1.5$ and width $b/R=0.5$. The arch thickness t/R is ranging from 0.025 to 0.25, and the embrace angle β from 90° to 180° . Buttresses are allowed to develop either horizontal or oblique ruptures.

t/R	SNBV horizontal rupture of buttress				SNBV oblique rupture of buttress				$\varepsilon = \frac{b}{h} = \frac{b}{R} \frac{R}{h}$	
	ε	φ_1 ($^\circ$)	φ_2 ($^\circ$)	φ_3 ($^\circ$)	ε	φ_1 ($^\circ$)	φ_2 ($^\circ$)	φ_3 ($^\circ$)		
	$\beta=90^\circ$				$\beta=125^\circ$					
0.025	0.278	64.57	104.16	135	0.177	59.61	99.71	135	0.421	0.333
0.05	0.244	55.73	101.39	135	0.143	50.87	97.20	135	0.416	
0.075	0.221	50.18	99.62	135	0.123	45.45	95.60	135	0.426	
0.1	0.205	46.26	98.42	135	0.111	45	94.65	135	0.441	
0.125	0.195	45	97.61	135	0.106	45	94.20	135	0.459	
0.15	0.190	45	97.16	135	0.106	45	94.05	135	0.478	
0.175	0.188	45	96.95	135	0.109	45	94.09	135	0.496	
0.2	0.189	45	96.92	135	0.115	45	94.26	135	0.514	
0.225	0.193	45	97.01	135	0.123	45	94.53	135	0.531	
0.25	0.198	45	97.21	135	0.133	45	94.88	135	0.547	
<hr/>										
$\beta=125^\circ$										
0.05	0.196	54.31	101.11	147.91	0.145	51.43	98.23	145.02	0.418	0.333
0.075	0.214	51.23	102.07	152.5	0.128	46.42	97.27	148.11	0.435	
0.1	0.198	47.43	101.17	152.5	0.118	42.99	96.75	150.50	0.455	
0.125	0.188	44.61	100.54	152.5	0.114	40.52	96.51	152.5	0.475	
0.15	0.183	42.47	100.13	152.5	0.114	38.70	96.46	152.5	0.493	
0.175	0.180	40.85	99.91	152.5	0.116	37.36	96.55	152.5	0.511	
0.2	0.180	39.63	99.82	152.5	0.121	36.40	96.73	152.5	0.527	
0.225	0.183	38.75	99.86	152.5	0.127	35.74	97.01	152.5	0.541	
0.25	0.187	38.14	99.99	152.5	0.134	35.34	97.36	152.5	0.555	
<hr/>										
$\beta=155^\circ$										
0.075	0.077	43.53	94.38	145.23	0.077	43.53	94.38	145.23	0.333	
0.1	0.188	46.91	100.67	154.42	0.112	42.65	96.41	150.16	0.432	
0.125	0.178	44.12	100.11	156.10	0.109	40.24	96.24	152.23	0.453	
0.15	0.172	42.01	99.78	157.55	0.110	38.48	96.25	154.02	0.472	
0.175	0.170	40.40	99.62	158.84	0.112	37.17	96.39	155.61	0.489	
0.2	0.169	39.19	99.60	160.00	0.116	36.22	96.63	157.04	0.504	
0.225	0.170	38.29	99.67	161.05	0.122	35.55	96.94	158.32	0.518	
0.25	0.173	37.64	99.82	162.00	0.128	35.12	97.30	159.48	0.530	
<hr/>										
$\beta=180^\circ$										
0.125	0.064	37.64	93.64	149.63	0.064	37.64	93.64	149.63	0.333	
0.15	0.144	40.44	98.21	155.99	0.093	37.53	95.30	153.07	0.421	
0.175	0.152	39.43	98.65	157.87	0.095	36.21	95.43	154.65	0.439	
0.2	0.151	38.17	98.58	158.99	0.099	35.24	95.65	156.05	0.454	
0.225	0.151	37.22	98.61	159.99	0.104	34.54	95.92	157.30	0.467	
0.25	0.153	36.53	98.71	160.89	0.109	34.05	96.23	158.41	0.479	

The rest of the process is identical to what has been presented earlier. The only difference is that in moment equilibrium equation of segment 1 (Eq. (3)) W_1 , x_1 and y_1 have changed due to the presence of the compression free area that does not participate in the mechanism (Alexakis and Makris 2017).

Fig. 10 and columns 6 to 9 of Table 1 offer the corresponding critical values presented in Fig. 7 and columns 2 to 5 respectively for the case where the buttress develops an elongation failure. The lines with the positive slope of Fig. 10 that represent the arch mechanism (mechanism I in Fig. 5) remain the same; while, the slightly horizontal lines of mechanism II reveal a significant reduction of the seismic capacity due to the oblique elongation failure. The 10th column of Table 1 presents the dimensionless distance z/h . Isolated symbols in Fig. 10 correspond to Discrete Element Method results discussed later.

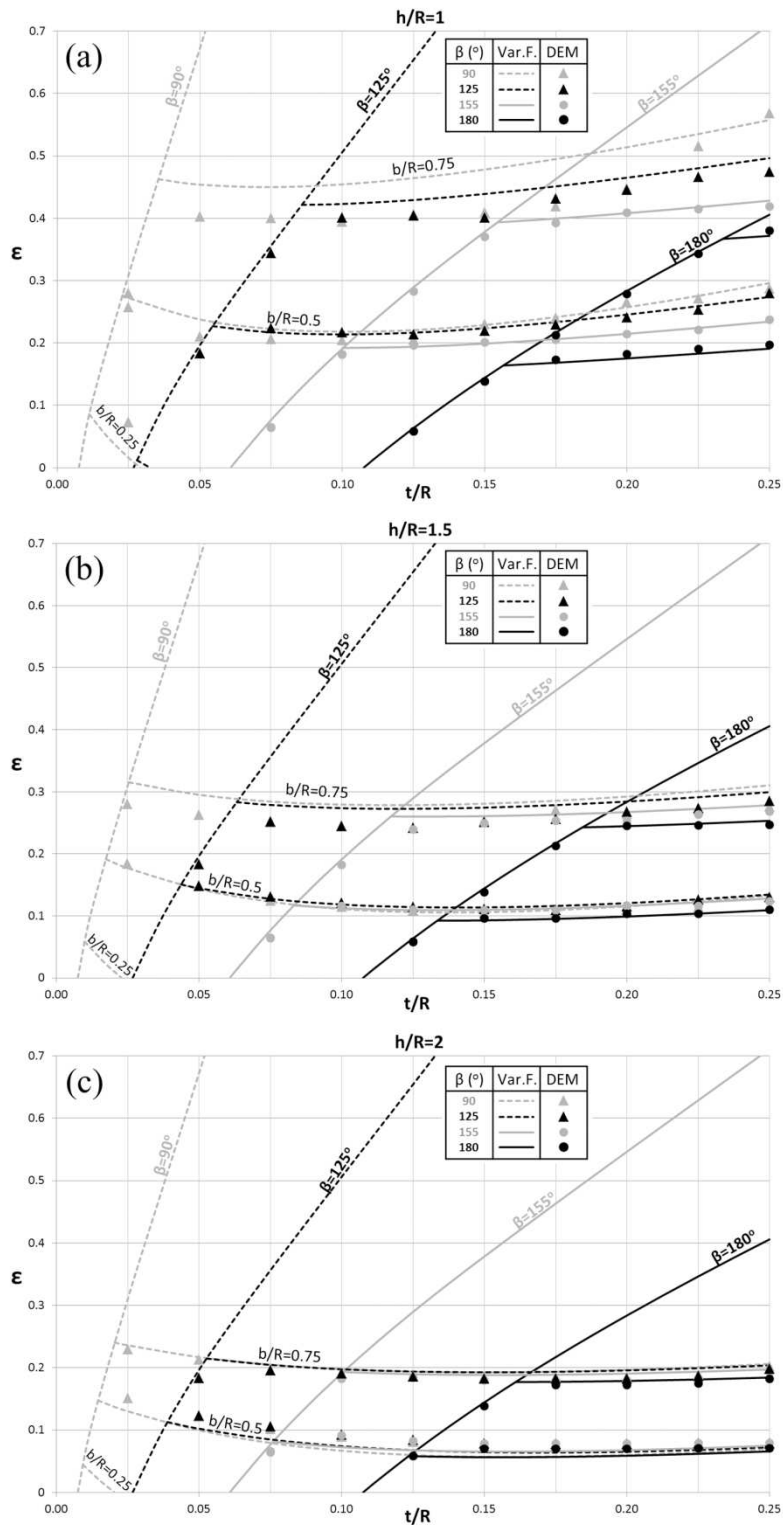


Figure 10. Seismic coefficient ϵ for different geometries of the single-nave barrel vault with buttresses that are allowed to develop an oblique elongation failure. Lines: Results from the variational formulation. Isolated symbols: Results from the Discrete Element Method (DEM).

VALIDATION OF THE DISCRETE ELEMENT METHOD (DEM)

Over the last two decades an increasing number of engineers are using the Discrete Element Method (DEM) for the analysis of masonry structures and monuments in an effort to capture the discontinuous nature of masonry (Cundall 1971, Pagnoni 1994, Lemos 1995, 2007, Papantonopoulos et al. 2002, among others). In this paper, the results presented in Figs. 7 and 10 are compared with the results obtained with DEM analysis, where the commercially available software UDEC (Universal Distinct Element Code – Itasca Consulting Group, Inc. 2004) has been used. Recently, Alexakis and Makris (2016) presented a validation of DEM for the limit stability analysis of masonry arches where DEM reproduces the analytical results with remarkable accuracy.

In order for the result of DEM to be comparable with those of limit equilibrium analysis, the stone blocks must be considered as rigid; whereas, the angle of friction between the joints, φ , must be large enough (e.g. $\varphi \geq 80^\circ$) to prevent sliding. In addition, the effect of the mortar has been neglected and the tensile strength, the cohesion and the dilatancy angle shall be zero.

The method adopts an elastic behavior which leads to the need to define the normal-to-the-contact surface, K_n (normal stiffness), and the tangential-to-the-contact surface, K_s (shear stiffness), equivalent linear elastic constants. The variation of these values has marginal effect for the assessment of the limit state that is the minimum seismic coefficient ε and the imminent hinging mechanism. By using values between 10^7 Pa/m and 10^9 Pa/m the algorithm converges fast and with reliable results. In this analysis $K_n=K_s=10^8$ Pa/m.

The material density does not appear in the equations of limit analysis, which is governed by geometry. The DEM confirms this behavior since very small or very large values of density have been tested without affecting the results of the limit equilibrium analysis. In this analysis the density was chosen to be 2000 kg/m 3 . Similarly, it was confirmed that the results of the analysis remain invariant to scale. It was chosen $R=1$ m.

Fig. 11 presents the discretized models that were used: (a) for the case where the buttresses are allowed to rupture horizontally at any height and (b) for the case where the buttresses are allowed to develop an oblique elongation failure. All voussoirs have size=5°, which means that the arches with embrace angle $\beta=180^\circ, 155^\circ, 125^\circ, 90^\circ$ have 36, 31, 25, 18 voussoirs respectively. The same discretization was used by Alexakis and Makris (2014) satisfactorily to reproduce the collapse mechanisms of circular arches under lateral and gravity loads. The gravity load and horizontal inertia load corresponding to each block are applied as static loads at the center of gravity of each block.

For case (a) all buttresses are divided into twenty identical rectangular blocks and one trapezoidal block at the head, as shown in Fig. 11(a). The circular and triangular points in Fig. 7 represent the results obtained with DEM for all the range of t/R values with step 0.025. The circular black dots correspond to the solid black line for $\beta=180^\circ$. The circular gray dots correspond to the solid gray line for $\beta=155^\circ$. The triangular black points correspond to the dashed black line for $\beta=125^\circ$. The triangular gray points correspond to the dashed gray line for $\beta=90^\circ$. The numerical solution of DEM is in excellent agreement with the theoretical solution from the variational formulation. It is confirmed that the buttress uplifts without developing any intermediate horizontal ruptures and the location of the 4 hinges match those predicted from the theoretical solution.

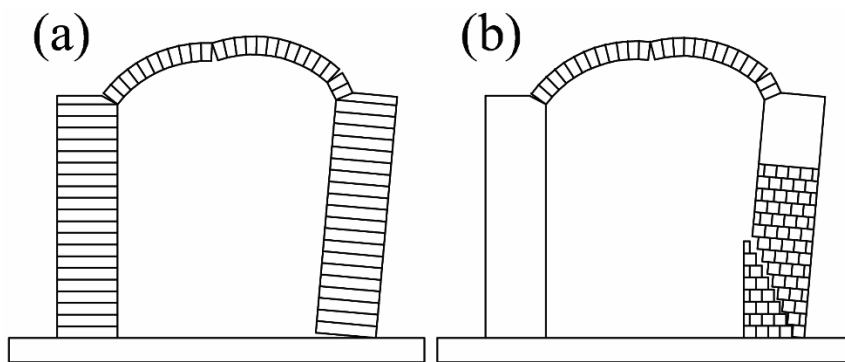


Figure 11. Models used in DEM analysis with: (a) buttresses that are allowed to develop horizontal ruptures only; and (b) buttresses that are allowed to develop an elongation failure.

For case (b) a finer discretization was chosen for the buttress in order to capture the diagonal failure, as shown in Fig. 11(b). In principle, the finer the discretization is, the better the elongation failure can be reproduced. However, for large number of blocks the algorithm does not converge. For this reason, given that the theoretical solution predicted that the distance $z/h > 0.38$, the upper 30% of the right buttress was not discretized together with the left buttress, where diagonal fracture is not expected. The size of the square blocks of the right buttress was chosen $0.1R$. The dots in Fig. 10 represent the results obtained with DEM. Given that there is a slight deviation between the exact area of the discretized buttress that uplifts compared with the theoretical one, the results are still in good agreement.

CONCLUSION

This paper examines and compares the minimum horizontal acceleration that is needed to initiate uplift of the single-nave barrel vault and of the rocking frame—the two most common masonry structural systems used to bridge a span.

Regarding the single-nave barrel vault, depending on the relative slenderness of the arch to the slenderness of the buttress, the paper identifies two lower failure mechanisms: (a) hinging of the arch alone—that is a mechanism where the buttresses do not participate as if the arch was supported on the ground; and (b) hinging of the arch together with a hinge at the base of the “downstream” buttress. In this analysis, radial ruptures are assumed for the arch; while, the buttress may rupture either horizontally or develop an oblique elongation failure along which the compression free portion of the buttress separates. In the event that the buttresses are built out of large masonry blocks and the rupture happens along a horizontal direction (entire buttress uplifts), the single-nave barrel vault ruptures with a seismic coefficient ε that is always smaller than the slenderness of the buttresses $=b/h$. As the embracing angle of the arch diminishes the single-nave barrel vault hinges at a higher value of the seismic coefficient, which however remains lower than the hinging seismic coefficient of the rocking frame which is $\varepsilon=b/h$. Accordingly, the rocking frame—that is two free-standing columns caged with a prismatic epistyle has always higher rupture acceleration, $\varepsilon=s=b/h$, than any configuration of the single-nave barrel vault with buttresses having the same slenderness, $s=b/h$.

REFERENCES

Alexakis, H., and Makris, N. (2013a). “Structural Stability and Bearing Capacity Analysis of the Tunnel-Entrance to the Stadium of Ancient Nemea”, *International Journal of Architectural Heritage: Conservation, Analysis, and Restoration*, 7(6), 673-692.

Alexakis, H., and Makris, N. (2013b). “Minimum thickness of elliptical masonry arches.” *Acta Mechanica*, 224(12), 2977-2991.

Alexakis, H., and Makris, N. (2014). “Limit equilibrium analysis and the minimum thickness of circular masonry arches to withstand lateral inertial loading.” *Arch. Appl. Mech.*, 84(5), 757-772.

Alexakis, H., and Makris, N. (2015). “Limit equilibrium analysis of masonry arches.” *Arch. Appl. Mech.*, 85(9), 1363-1381.

Alexakis, H., and Makris, N. (2016). “Validation of the Discrete Element Method for the Limit Stability Analysis of Masonry Arches.” *Computational Modeling of Masonry Structures Using the Discrete Element Method*, IGI Global, 292-325.

Alexakis, H., and Makris, N. (2017). “Hinging Mechanisms of Masonry Single-Nave Barrel Vaults Subjected to Lateral and Gravity Loads.” *J. Struct. Eng.*, 143(6), 04017026-1-04017026-11.

Clemente, P. (1998). “Introduction to dynamics of stone arches.” *Earthq. Eng. & Struct. Dyn.*, 27(5), 513-522.

Cundall, P. A. (1971). “A computer model for simulating progressive large-scale movements in blocky rock system.” *Proc. of the Symposium of the Int. Soc. for Rock Mechanics*, Vol. 1, Nancy, France, paper no II-8.

De Lorenzis, L., DeJong, M., and Ochsendorf, J. (2007). “Failure of masonry arches under impulse base motion.” *Earthq. Eng. & Struct. Dyn.*, 36(14), 2119-2136.

Heyman, J. (1992). “Leaning Towers.” *Meccanica*, 27, 153-159.

Huerta, S. (2006). “Galileo was Wrong: The Geometrical Design of Masonry Arches.” *Nexus Netw. J.*, 8(2), 25-52.

Itasca Consulting Group, Inc. (2004). *UDEC: Universal Distinct Element Code*, Version 4.0, Itasca, Minneapolis.

Lagomarsino, S. and Cattari, S. (2015). “PERPETUATE guidelines for seismic performance-based assessment of cultural heritage masonry structures.” *Bull. Earthq. Eng.*, 13(1), 13-47.

Lemos, J. V. (1995). “Assessment of the ultimate load of a masonry arch using discrete elements.” *Computer Methods in Structural Masonry*, Books & Journals International, Swansea, 294-302.

Lemos, J. V. (2007). “Discrete element modelling of masonry structures.” *Int. J. Arch. Her.*, 1(2), 190-213.

Makris, N. (2014a). “The Role of the Rotational Inertia on the Seismic Resistance of Free-Standing Rocking Columns and Articulated Frames.” *Bull. Seism. Soc. Am.*, 104(5), 2226-2239.

Makris, N. (2014b). “A half-century of rocking isolation” *Earthquakes and Structures*, 7(6), 1187-1221.



Makris, N., and Alexakis, H. (2012). "From Hooke's "Hanging Chain" and Milankovitch's "Druckkurven" to a variational formulation: The adventure of the thrust-line of masonry arches", *Report series in EEAM 2012-02*, University of Patras, Greece.

Makris, N., and Alexakis, H. (2013). "The effect of stereotomy on the shape of the thrust-line and the minimum thickness of semicircular masonry arches." *Arch. Appl. Mech.*, 83(10), 1511-1533.

Makris, N., and Alexakis, H. (2015). "Limit equilibrium analysis of masonry buttresses and towers under lateral and gravity loads." *Arch. Appl. Mech.*, 85(12), 1915-1940.

Makris, N. and Vassiliou, M. F. (2013). "Planar rocking response and stability analysis of an array of free-standing columns capped with a freely supported rigid beam." *Earthq. Eng. & Struct. Dyn.*, 42(3), 431-449.

Makris, N. and Vassiliou, M. F. (2014). "Are Some Top-Heavy Structures More Stable?" *J. Struct. Eng.*, 140(5).

Ochsendorf, J. (2002). "Collapse of masonry structures." *Doctoral dissertation*, Department of Engineering, University of Cambridge, U.K.

Ochsendorf, J. A., Hernando, J. I., and Huerta, S. (2004). "Collapse of masonry buttresses." *J. Archit. Eng.*, 10(3), 88-97.

Oppenheim, I. J. (1992). "The masonry arch as a four-link mechanism under base motion." *Earthq. Eng. & Struct. Dyn.*, 21(11), 1005-1017.

Pagnoni, T. (1994). "Seismic analysis of masonry and block structures with the discrete element method." *Proc., 10th European Conf. on Earthq. Eng.*, Vol. 3, Balkema, Rotterdam, 1669-1674.

Papantonopoulos, C., Pscharis, I. N., Papastamatiou, D. Y., Lemos, J. V., and Mouzakis, H. P. (2002). "Numerical prediction of the earthquake response of classical columns using the distinct element method." *Earthq. Eng. & Struct. Dyn.*, 31(9), 1699-1717.

Roca, P., Cervera, M., Gariup, G., and Pela', L. (2010). "Structural Analysis of Masonry Historical Constructions. Classical and Advanced Approaches." *Arch. Comp. Meth. Eng.*, 17(3), 299-325.

Shames, I. H., and Dym, C. L. (1985). *Energy and Finite Elements Methods in Structural Mechanics*, Hemisphere Publishing Corporation, New York.



INTERNATIONAL JOURNAL OF
**GEOENGINEERING
CASE HISTORIES**

*The Journal's Open Access Mission is
generously supported by the following Organizations:*



Geosyntec
consultants

engineers | scientists | innovators

CONETEC



ENGEO
Expect Excellence

Access the content of the ISSMGE International Journal of Geoengineering Case Histories at:
<https://www.geocasehistoriesjournal.org>